Synthesising Lead Oxide and Oxychloride Minerals from Spent Lead Acid Battery Waste using a Choline-Chloride based Deep Eutectic Solvent

Enrico W. Manfredi-Haylock,[1,*] Gwilherm. K. Kerherve,[1] David J. Payne [1]

[1] Department of Materials, Imperial College London, Exhibition Road, London SW7 2AZ, U.K.

* Corresponding Author

Keywords

Lead Acid Batteries, Recycling, Deep Eutectic Solvent

Abstract

Lead acid batteries have been successfully recycled with pyrometallurgy for many years. However, this process has historically been associated with mass lead poisonings and continues to contribute significantly to disease burden in developing nations. In this paper a cleaner alternative to pyrometallurgical processing is proposed using deep eutectic solvents (DES) based on choline chloride and oxalic acid to dissolve and convert lead materials into pure lead oxalate which can then be calcined at low temperatures into lead oxide products that can be used for the synthesis of new batteries. We also show that lead oxychlorides can be formed at lower calcination temperatures due to the presence of residual chlorine from the DES.

Highlights

- Desulphurised spent lead acid battery paste was reacted with Oxaline, a Deep Eutectic Solvent (DES) composed of a 1:1 molar ratio of choline chloride and oxalic acid.
- All lead materials in the desulphurised spent lead acid battery paste were converted into lead oxalate.
- Lead oxalate begins to decompose at 400°C into lead oxychloride compounds due to the presence of chlorine from the DES
- This study establishes the importance of using chlorine-free solvents if the objective is to calcine lead oxalate into pure lead oxide for new lead acid battery manufacture.

1. Introduction

1.1 The Impact of Lead Recycling

The lead acid battery (LAB) is a ubiquitous and essential piece of modern technology that allows for cheap storage of large amounts of electrical power. Starting, lighting and ignition (SLI) batteries are used in every automobile currently on the road [1] while deep-cycle batteries are mostly used for stationary energy storage applications for electrical infrastructure [2]. Currently LABs are the most recycled product in the world and are recycled to almost 100% efficiency in OECD nations [3]. However there still exist two main problems with the way that LABs are currently recycled. Firstly, the dominant process (pyrometallurgy) requires smelting at >1000 °C to reduce lead materials in the spent LAB paste into metallic lead that can be resold. This results in a process energy requirement of over 1000 kWh per tonne of lead produced. The power requirements of heating are such that fossil fuels are commonly used to power the smelter units and therefore this translates to the production of 550kg of CO_2 per tonne of lead recycled [4]. Secondly, unless suitable emission control measures are in place, the recycling process is highly polluting and can lead to local environmental and water contamination due to lead particulate emissions. Poorly regulated recycling activities are well documented to cause mass poisonings, particularly in developing nations where batteries are recycled informally [5].

1.2 Innovations in Lead Recycling

Solution-based recycling methods have recently been gaining attention both from academia and industry. These possess the key advantages in that they do not fume lead particulates like smelting does (as all lead is trapped in solution) and typical operating temperatures of the process are around 100°C, leading to energy savings. Early methods of liquid LAB recycling were based on the Betts electrowinning method [6] where H_2SiF_6 (hexafluorosilic acid) or HBF_4 (tetrafluoroboric acid) are used to dissolve the lead compounds. An electrostatic potential is then used to deposit pure metallic lead on the cathode. A significant drawback of these methods is the cost, and the chemical hazard of these powerful acids, that can evolve HF if the correct additives are not present in the solution [7]. Electrochemical processes involving less hazardous chemicals have since been developed, for example the LEDCLOR process developed by Técnicas Reuinidas use mixtures of HCl and brine [8] while Aquametals Inc. have developed a methanesulphonic/EDTA processing solution [9]. However, the drawback of all these methods is the high electrical energy consumption, which is the same or exceeding the fossil fuel equivalent of pyrometallurgy. This makes these alternative processes economically unattractive since the energy cost alone far

exceeds that of traditional smelting due to the higher costing of electrical energy from the grid compared to a typical fossil fuel such as natural gas [10].

Recently some purely chemical methods for LAB recycling have been developed to circumvent this issue. Leaching and cementation reactions have been proposed using HCl by Técnicas Reuindas (known as the PLINT process) [11], acetic acid over a metallic iron surface[12], and citric acid [13]. All these processes produce an intermediate lead compound that must undergo further processing to be made into a product that can be used in battery manufacturing. These products are thermally processed at much lower temperatures than smelting (< 500 °C), yielding significant energy savings against traditional pyrometallurgy. The downside of these methods is that (a) they use a lot of water in the aqueous processing solutions and (b) the lead recovery rate can be low even over a period of days. A low recovery and slow speed of reaction affects efficiency and throughput, which are key success factors in the lead recycling industry. Heavy water use in such a large industry will also make future water shortages worse [14] especially in nations of the Global South where changes to the recycling process are most crucially needed.

A new chemical and electrochemical recovery method using non-aqueous solvents is currently being explored [15], [16] where a novel class of sustainable ionic liquid analogues known as deep eutectic solvents (henceforth referred to as DES) are used to dissolve and convert a wide variety of lead materials. Like ionic liquids, these solvents show exceptional reactivity and are able to process even stable metal oxides, but unlike ionic liquids, their synthesis is both facile and inexpensive [17]. A common deep eutectic solvent known as Ethaline 200 is a simple mixture of choline chloride and ethylene glycol in a 1:2 molar ratio and is synthesised by stirring at 80 °C until it forms a colourless liquid [18]. Proof of concept work for the electrochemical recovery of lead using this solvent has been carried out for both lead perovskite materials [19] and spent LAB paste [15] has shown promising initial results, and a new chemical process based on deep eutectic solvents is proposed.

While the above proof of concept work recovers lead electrochemically, this work proposes a new, purely chemical method of lead material recovery using a new type of DES. This DES is composed of a 1:1 molar ratio of choline chloride and oxalic acid dihydrate. The synthesis of this solvent is as simple and inexpensive as that of the Ethaline 200 solvent while the chemical reactivity with lead compounds is significantly higher even at room temperature. This purely chemical process yields lead (II) oxalate which can be theoretically processed into lead (II) oxide at less than 400°C in 2 hours. The advantages of such a process would be (a) no electricity or heating being required to convert spent lab materials to lead (II)

oxalate, (b) fast conversion of a mixed stream of lead compounds into a single intermediate product and (c) the circumvention of a reductive step to obtain lead metal, as the end material should be ready to use in “leady oxide” which is used to make new batteries [20].

The first aim of this study is to confirm the identity of the input, intermediate and output materials of this process. The input material investigated was desulphurised lead paste with unknown composition, while the intermediate material and output materials require characterisation. The second aim of this study was to find the lowest possible calcination temperature for the intermediate material to obtain the final useful product of lead (II) oxide. To do this, calcination at 500,400 and 300°C and the resulting output materials were characterised. All materials where characterised using XPS, XRD and SEM/EDX.

2. Experimental

The DES was prepared by mixing choline chloride (Sigma > 98.0%) and oxalic acid di-hydrate (Sigma > 99.0%) on a heated magnetic stirring plate at 50 °C and 300 revolutions per minute (henceforth abbreviated to rpm) until a homogeneous clear liquid is formed. 5.5 mg of desulphurised spent LAB paste (provided by Envirowales Ltd.) was added per ml of DES prepared, and the solution was agitated with a magnetic stirrer set to 500 rpm at room temperature for 24 hours. A suspension is formed and 35ml is transferred to a 50 ml conical tube to be centrifuged in an Eppendorf 5804 centrifuge for 30 minutes at 5300 rpm. The precipitate is then washed in three steps. Firstly, the supernatant is decanted, and the precipitate is re-suspended in oligo-ethylene glycol (m_w ~ 200, Sigma) and centrifuged at 5300rpm for 30 minutes. Then the supernatant is decanted, and the precipitate is then re-suspended in distilled (19 µS/cm) water and centrifuged at 5300rpm for 30 minutes. Lastly, the supernatant is decanted, and the precipitate is re-suspended in acetone and centrifuged at 5300rpm for 30 minutes. After the third step the supernatant is decanted, and the precipitate is transferred to a small vial and air dried in a Büchi B-585 glass oven overnight at 140 °C. The precipitate was then calcined at 300 and 500 °C in air with a 10 °C/minute heating rate. Each sample was held at the final temperature for 1 hour in an Elite Thermal Systems TSH12/38/250 tube furnace, using a 20 ml alumina crucible and silica tube.

The spent LAB paste, chemically converted product and calcined samples were investigated with XPS, PXRD to analyse the surface and bulk compositions respectively, while SEM was used to analyse differences in surface morphology. Compositional information of certain local points of interest on the surface were also analysed using energy dispersive x-ray

spectroscopy (EDX). Image analysis of fibres in secondary electron images was conducted on ImageJ by applying a black and white threshold and edge detection to the image. Fibres exhibited charging and therefore had higher white values which were set as the threshold to ensure that only fibres were detected by the black and white masking algorithm. Additionally, only objects with an aspect ratio greater than 2 were selected for counting. The resulting detected fibres were then modelled as ellipses with the semi-major axis representing the length and semi-minor axis representing the width of the fibre.

XPS was conducted in a Thermo Fisher K-alpha high throughput system using a 180° double focussing hemispherical analyser with an area detector, 400 µm x-ray spot size using an Al-Kα cathode source. Nominal analysis chamber pressure was set to $2x10^{-8}$ mbar before the start of the experiment. Samples were mounted onto a tantalum slide with carbon tape as fine powders. Spectra were analysed using the integrated Avantage software suite. Tougaard backgrounds were used on all core levels and the peaks were fitted with a non-linear chi square minimisation algorithm. The energy scales were calibrated with reference to the adventitious carbon peak which was set to 284.8eV. An ion flood gun was used to prevent sample charging.

PXRD was conducted with a Panalytical X'Pert x-ray diffractometer with standard goniometer geometry using a nickel-filtered Cu-Kα cathode source. Spectra were acquired between 5 and 80° 2θ with angular step size of 0.016° and an integration time of 20s. Samples were mounted as fine powders into a zero-diffraction silicon disk holder covered with mylar film to prevent sample spillage. This was found to present a significant peak at around 25° (2θ) due to its crystallinity. Therefore a reference pattern for the mylar film was collected and subtracted from the sample patterns to allow for qualitative phase analysis. Data was processed with the integrated Panalytical Highscore analysis suite.

SEM was conducted on a JEOL6010LA using a tungsten filament and with an integrated EDX and backscatter sensor. All images were taken with at 15kV accelerating voltage, a working distance of 21mm and a spot size of 40nm. Samples were mounted as fine powders to an aluminium stub with carbon tape.

3. Results & Discussion

3.1 Desulphurised Lead Acid Battery Paste Characterisation

The starting material used in this work was desulphurised lead paste provided by Envirowales Ltd. This was analysed by XRD, XPS and SEM to determine the morphology and lead compounds present. The XRD pattern for this material is shown in Figure 1. The most significant components are α-PbO (litharge, ICSD 62842), $PbCO_3$ (cerrusite, ICSD 6178) and $NaOH(PbCO_3)_2$ (abellaite, ICSD 261807). These products are common in lead paste that has been desulphurised in $NaHCO_3$ at high temperatures [21].

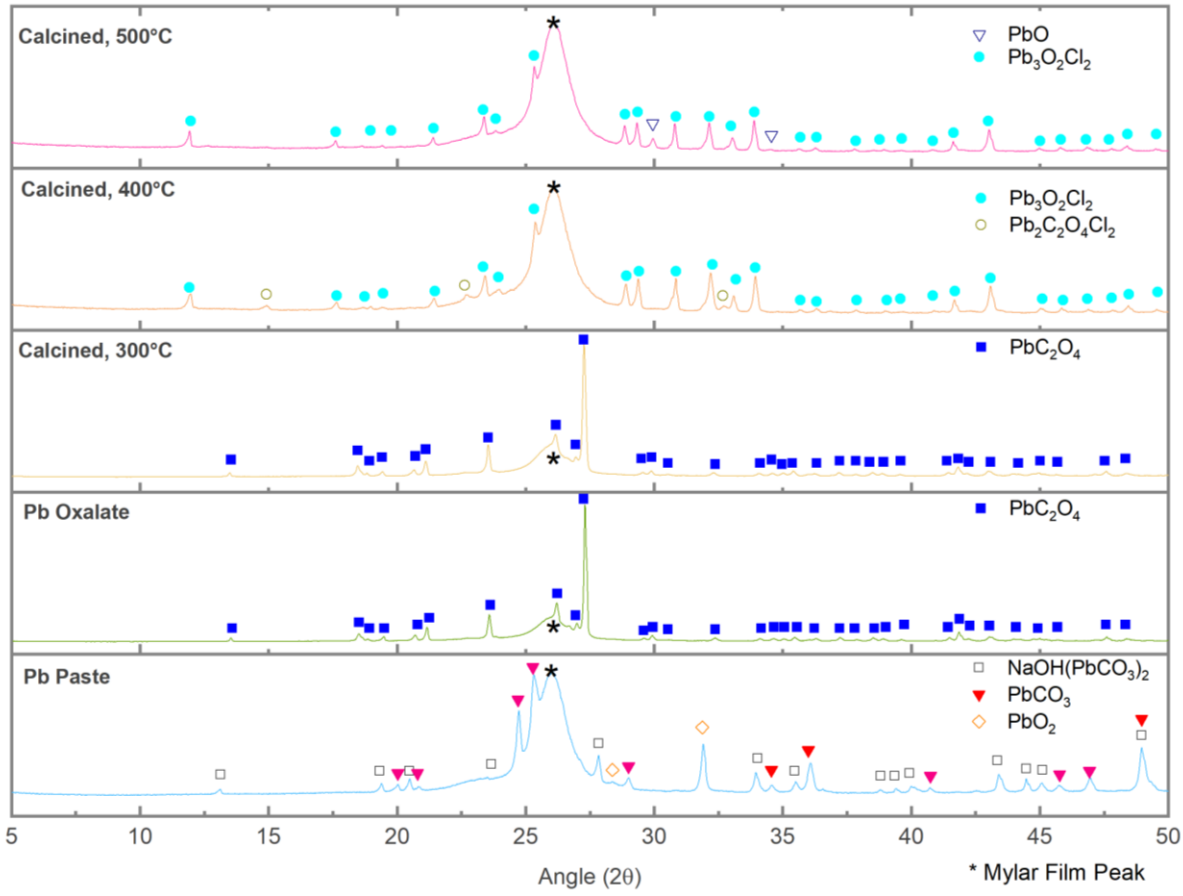

Figure 1: XRD patterns of (bottom to top) the as provided desulphurised lead acid battery paste, the converted product after reaction with ChCl:Oxalic Acid DES, the product after 300°C calcination in air, the product after 400°C calcination in air and the product after 500°C calcination in air.

This result is correlated by XPS measurements shown in Figure 2. The XPS survey reports the presence of Pb, Na, O, C and Si. Two lead environments are measured in the *Pb 4f* core level and are attributed to $NaOH(PbCO_3)_2$ or $PbCO_3$ [22] (138.5 eV) and PbO (137.3 eV) respectively. The single Na environment in the *Na 1s* core level at 1072.2 eV is attributed to $NaOH(PbCO_3)_2$. A single Si environment in the *Si 2p* at 102.7 eV is attributed

to SiO_2 [23]. The *O 1s* core level was found to have three resolvable environments and these are assigned to SiO_2 (532.8 eV) [23], $NaOH(PbCO_3)_2$ / $PbCO_3$ (531.4 eV) [22] and PbO or adventitious organic C-O (529.6 eV) [24]. The *C 1s* core level was found to have 3 environments assigned to C-C (set to 284.8eV), C-O (286.5 eV) and C=O (289.2 eV) which are all assigned to adventitious carbon compounds. The C-O and C=O may also contain signal from the carbonate species identified in the Pb core level and XRD. The integrated peak areas of environments relating to $NaOH(PbCO_3)_2$ in the *Na 1s*, *Pb 4f* and *O 1s* core levels were found to be in a 1:2.1:7.2 ratio respectively. Even though $PbCO_3$ was also measured by XRD, it is likely that only $NaOH(PbCO_3)_2$ is present at the surface due to the surface sensitivity of XPS and the close stoichiometric match of the core level ratios. The integrated peak areas of the environments relating to SiO_2 in the *Si 2p* and *O 1s* core levels were found to be in a 1:2.6 ratio, which only deviates slightly from expected stoichiometry. This deviation may be due to surface hydroxyl groups because of exposure to strongly alkaline conditions during the desulphurisation process. The integrated peak areas of environments related to PbO_2 in the *Pb 4f* and *O 1s* core levels were found to be in a 1:3.2 ratio which deviates from the expected 1:2 stoichiometry. From the survey spectrum a Zn 2p environment is also seen and therefore the presence of ZnO (which manifests in a similar range to PbO_2 O 1s environments at ~530.5 eV).

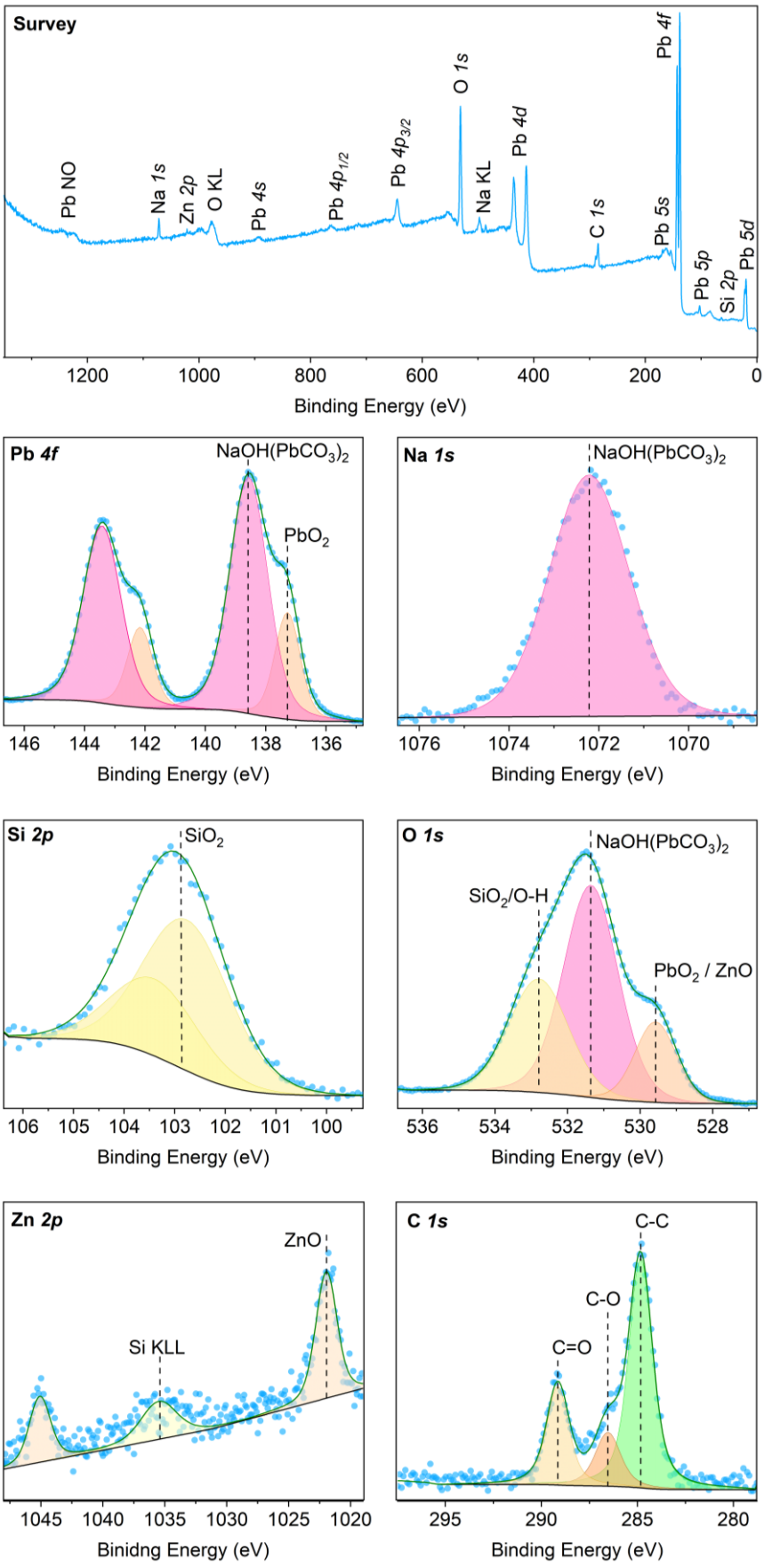

209

210 Figure 2: *XPS Survey and Pb, O, Na and Si core levels for the desulphurised lead acid*
211 *battery paste material.*

In SEM, large aggregates of material and bright streaks were observed (see Figure 3). The latter appeared to be fibres. These morphological features were investigated by EDX on the same electron microscope in Figure 4. It can be seen from these results that there is a strong spatial correlation between the aggregate material and the Pb M characteristic X-ray signal. Meanwhile the fibres show a positive spatial correlation with Si K and O K signal and an inverse spatial correlation with the Pb M signal. With reference to the XPS measurements, these fibres are SiO_2. The fibres were further size classified, and the results of this classification are shown in Figure 5. Both the length and diameter of the fibres show an exponential distribution from the smallest size of 10 µm diameter and 50 µm in length to the largest of 100 µm in diameter and 400 µm in length. These likely come from adsorbed glass mat (AGM) batteries that use woven silica fibres to immobilise the acid electrolyte [25]. Silica fibres from these batteries are difficult to separate from battery paste material during flotation and this indicates that AGMs make up a proportion of the batteries recycled in the batch of provided LAB paste.

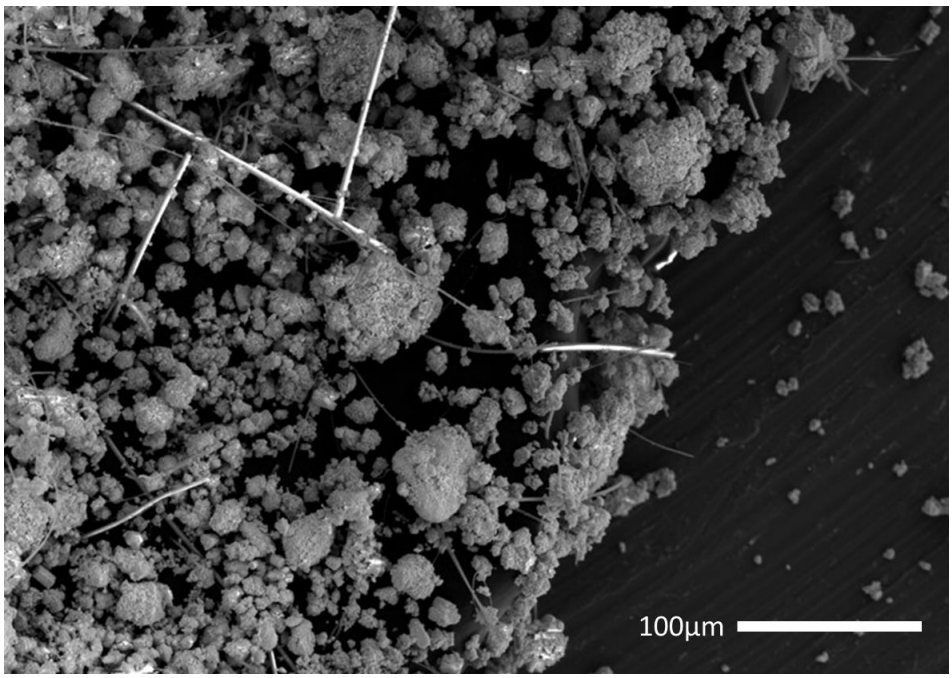

Figure 3: *Low magnification secondary electron image of the desulphurised paste surface.*

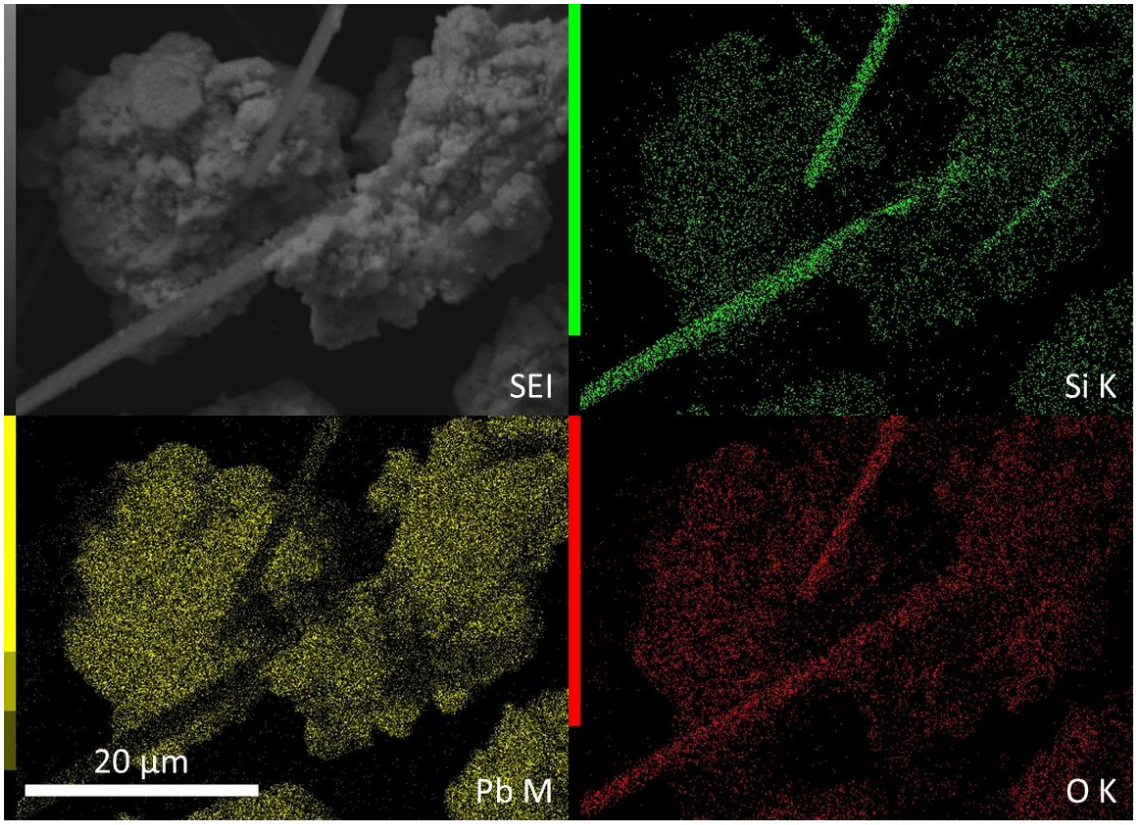

Figure 4: EDX area map and secondary electron image of aggregates and fibres.

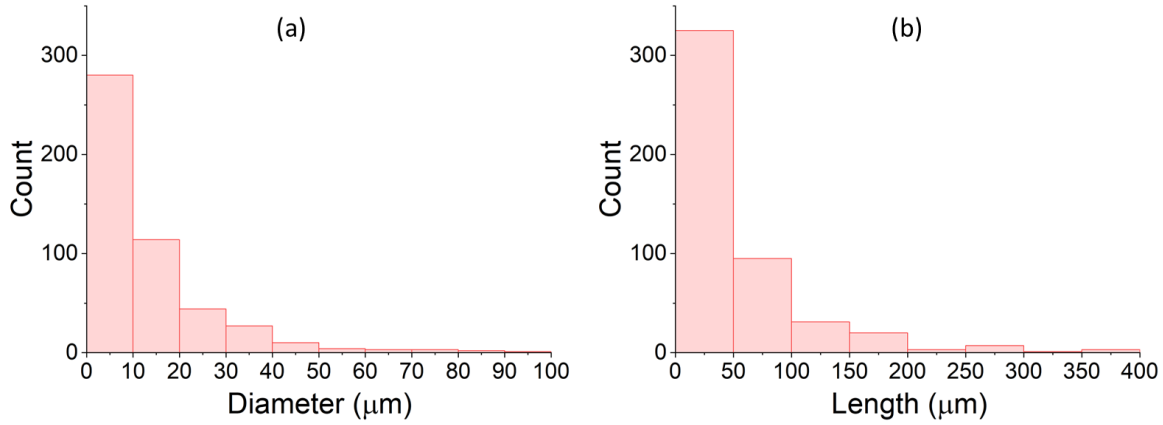

Figure 5: Histograms of classified fibre diameters (a) and lengths (b).

3.2 Chemical Conversion of Paste

Once spent LAB paste is added to the DES, paste granules transform into a white suspension over 24 hours of mixing. After this, the conversion is complete, and a fine white powder is obtained once the product is cleaned and dried. PXRD (see Figure 1) and XPS (see Figure 6) analyses confirm the product to be mainly comprised of PbC_2O_4 (lead

oxalate, ICSD 109830). It is interesting to note that while the PXRD pattern indicates the presence of mixed lead oxalate chloride species $Pb_2Cl_2C_2O_4$ (lead chloroxalate, ICSD 99805), XPS analysis failed to detect any chlorine in this product. This discrepancy between PXRD and XPS, indicates that $Pb_2Cl_2C_2O_4$ species can be found in the bulk but not at the surface. XPS analysis shows that the Na signal is not observed survey scan, and very different environments are present in the O *1s*, C *1s* and Pb 4*f* core levels. While a Pb metal environment (at 136.5eV) is still present in the Pb 4f core level, the only other environment present is shifted up to 138.79eV which is typical of organic lead compounds.[26] A dominant O 1s environment at 531.7 eV can be associated to this organic lead compound, and the only other O 1s environment at 533.4 eV is likely from SiO_2, since Si *2p* core level position remains unchanged compared to the input material. Finally, the C 1s peak associated with C=O at 288.54eV is much more intense than the LAB paste measurement and is even more intense than C-C peak at 284.8eV. Therefore, since this environment's signal is more intense than that of adventitious carbon compounds, it is assumed that this environment is part of the organic lead compound formed in this product. The Pb 4f: C(=O) 1s : O 1s ratio was found to be 1:2.3:4.6, in reasonable agreement with the PXRD identification of PbC_2O_4 as the major component of the product. The product was also imaged (shown in Figure 7) by SEM, and the crystal shape was noted to be plate-like with many crystal platelets sitting atop one another. This stacking of crystals is also observed in the PXRD measurement from the very high intensity of the 23.54° 2θ peak. This peak corresponds to the (002) plane of triclinic PbC_2O_4 crystals, and therefore suggests that crystal platelets preferentially align in the z direction (i.e. normal to the sample surface), as is seen in SEM.

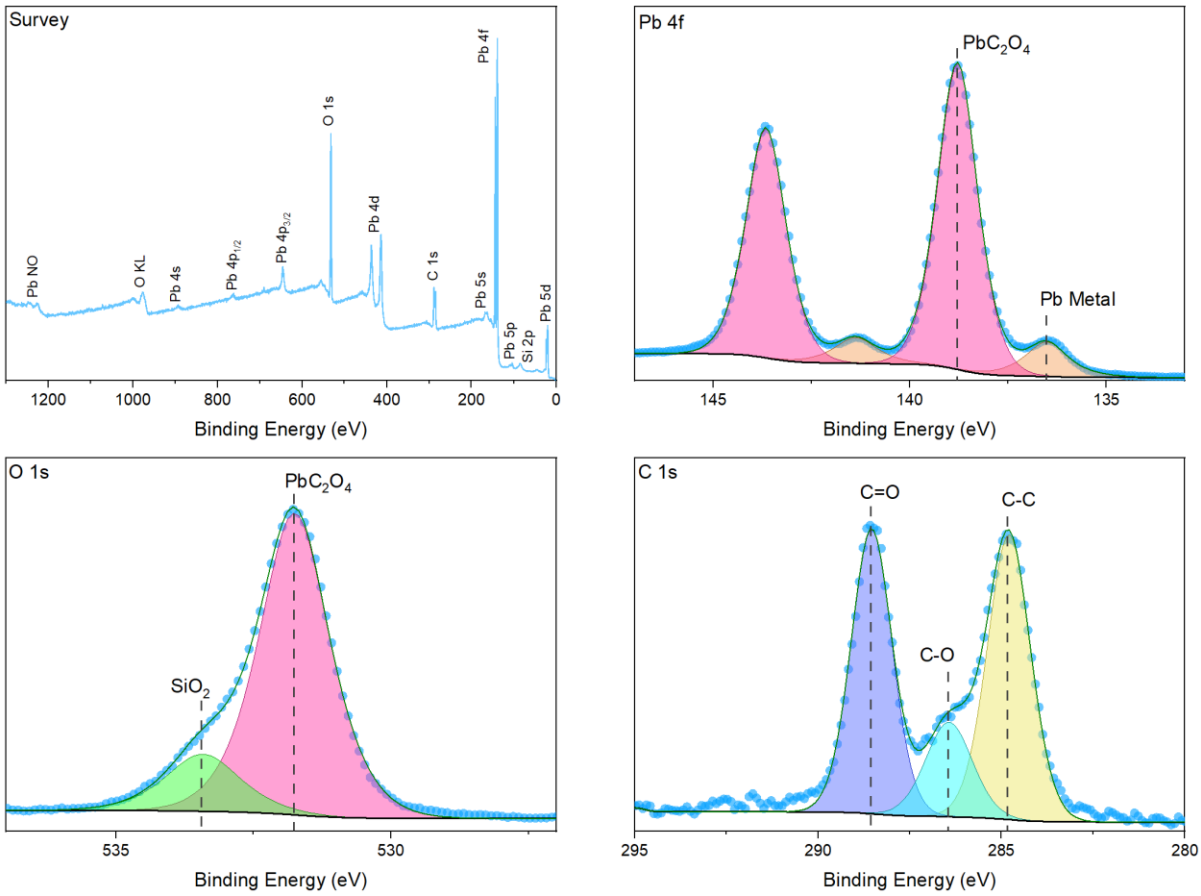

Figure 6: XPS analysis of chemically converted LAB paste. Survey spectrum of the product showing detected elements. A survey spectrum and core level spectra of Pb4f, C1s and O1s.Data points of core level measurements are shown as blue dots, while the fitted environment peaks are shown as filled areas under the envelope (green).

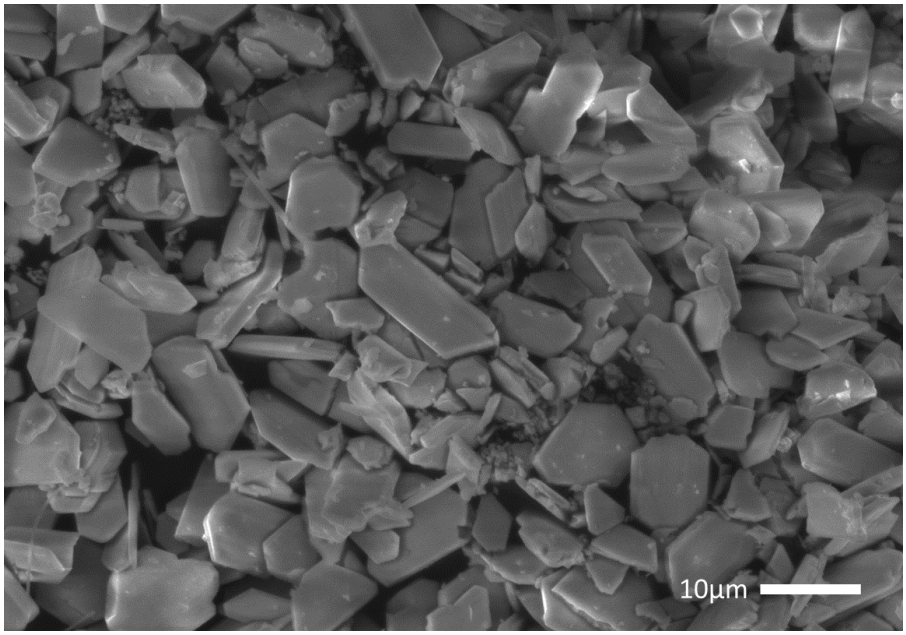

Figure 7: Secondary electron image of the powder obtained after the chemical conversion of spent LAB paste.

3.3 Calcination

After being calcined at 300°C, a grey powder was recovered. PXRD analysis (see Figure 1) and SEM (see Figure 8a) show the sample to be effectively unchanged compared to the original product of chemical conversion. Some subtle differences in peak intensities suggest that crystal alignment and packing has been disturbed by the calcination process. Crystals also appear to be less aligned when investigated with SEM due to some growth of small rectangular crystals between the larger platelets (shown in Figure 8b). XPS analysis (see Figure 9) however shows more pronounced changes at the surface. Chlorine is detected in the survey spectrum; however core level intensity ratios indicate that this is in the form of a $PbCl_2$ compound rather than $Pb_2Cl_2C_2O_4$ as measured in PXRD. These intensity ratios are taken between the Cl $2p_{3/2}$ environment at 198.05eV and the Pb $4f_{7/2}$ environment at 137.69eV. This environment is not observed in any other measurements and was therefore associated with the new Cl 2p peak. A more intense peak associated with a metallic lead environment at 136.43eV is also detected in the Pb 4f level at an atomic concentration of 2.6%. These observations are consistent with the early decomposition products of $Pb_2Cl_2C_2O_4$, where small amounts of lead chloroxalate convert to $Pb_5O_2Cl_6$, and some material may be converted to Pb metal by the presence of reducing agents in these products (such as CO). [27]

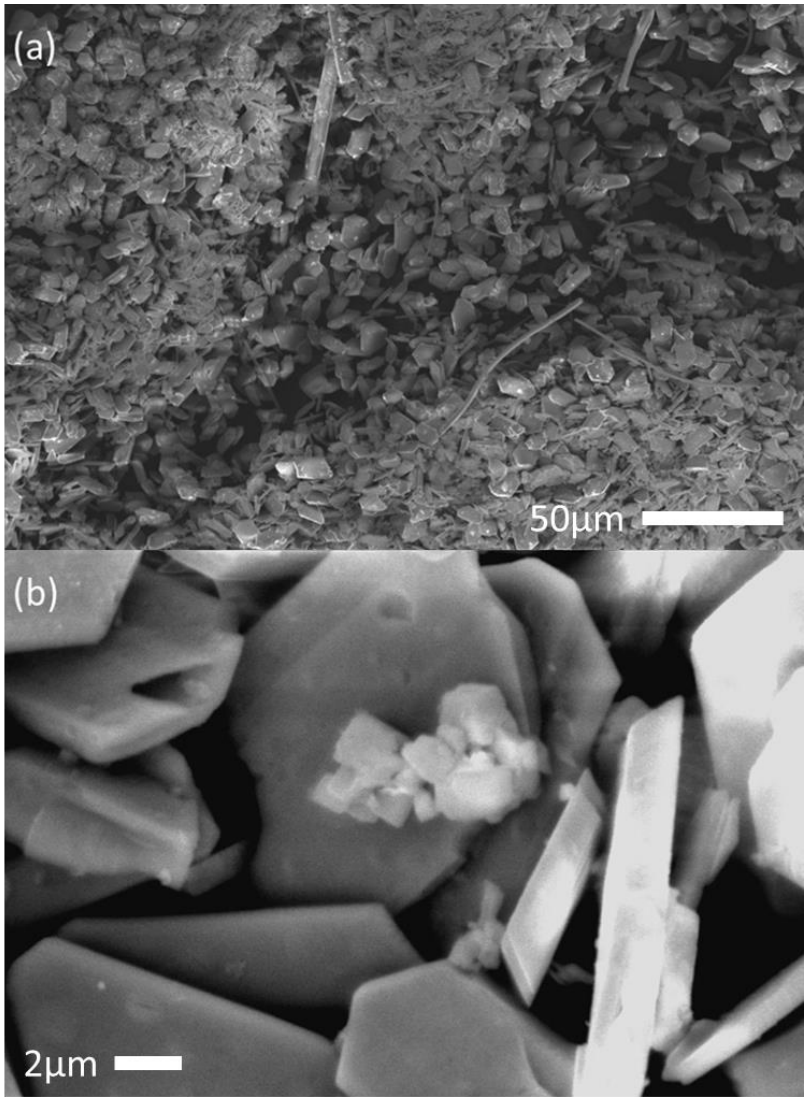

Figure 8: Investigation of surface morphology of PbC_2O_4 calcined at 300°C with (a) a low magnification secondary electron image and (b) high magnification image of a new phase identified growing between PbC_2O_4 platelets.

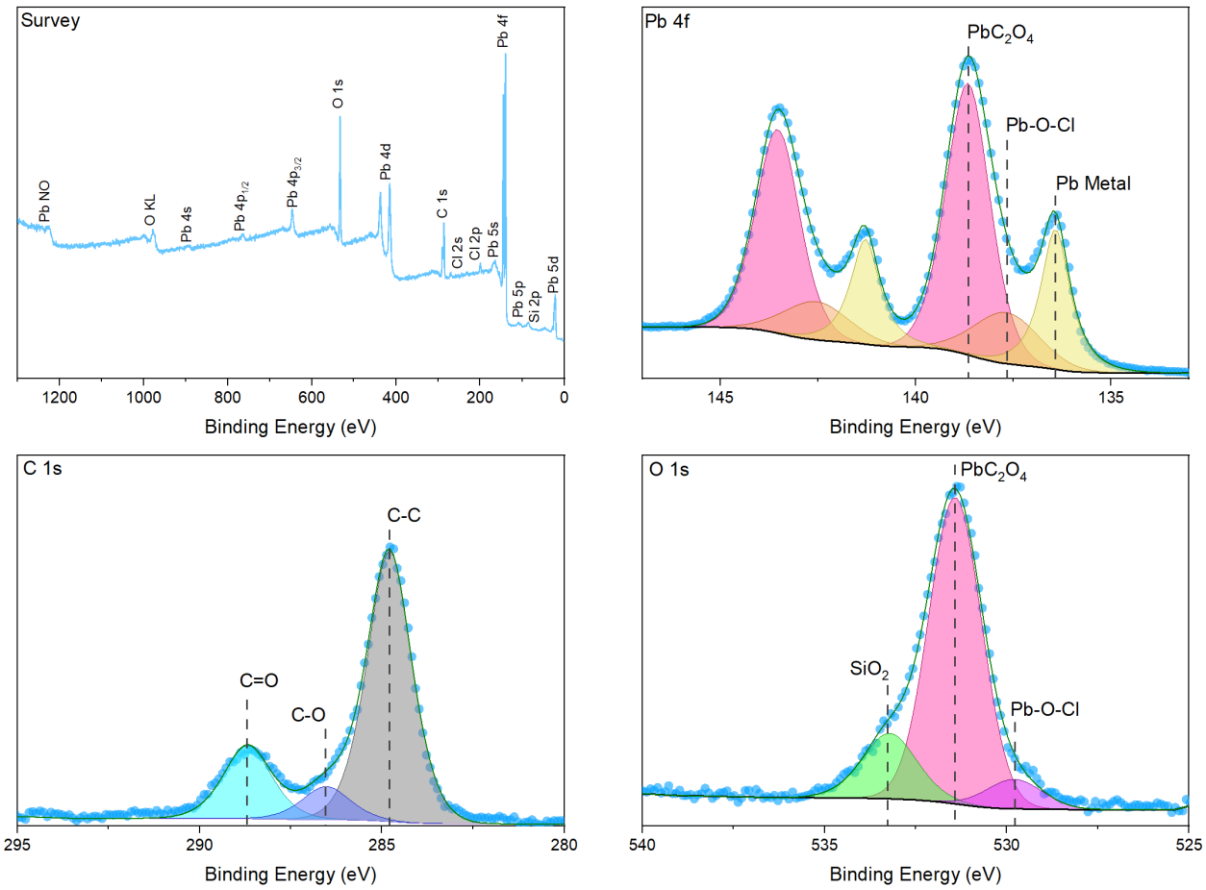

Figure 9: XPS analysis of chemically converted after calcination at 300°C. Survey spectrum of the product showing detected elements. A survey spectrum and core level spectra of Pb4f, C1s and O1s. Data points of core level measurements are shown as blue dots, while the fitted environment peaks are shown as filled areas under the envelope (green).

This decomposition pathway discussed in a thermal decomposition study of $Pb_2Cl_2C_2O_4$ by Boudaren et al.[27] Even though one would expect any free lead metal to oxidise during calcination, lead's slow oxidation kinetics at 300°C [28] make the observation of some residual metal likely. It is noted by Boudaren et al. that the formation of $PbCl_2$ would also be expected at low temperatures due to the presence of some Cl_2 in the decomposition gases and its reaction with metallic lead. The composition ratios observed between Pb 4f, Cl 2p and O 1s environments that are related to oxy-chloride compounds in XPS core level analysis could be explained by a mixture of overlapping $Pb_5O_2Cl_6$, $PbCl_2$ and $Pb_3O_2Cl_2$ environments, but more data is needed to determine the exact composition of this environment.

At a higher temperature of 500°C a white powder is recovered after calcination and a dramatic change can be seen in PXRD (see Figure 1), XPS and SEM (see Figure 10). PXRD shows that only one phase of an oxy-chloride mineral ($Pb_3O_2Cl_2$) is present, while

XPS shows a Pb:Cl ratio of 0.98:1 indicating that there may be mixed and overlapping Pb-Cl environments, as with the 300˚C calcined product, although with the significant difference that the compositional ratios between Pb and Cl are reversed, and the peaks associated with these environments are shifted. The Pb 4f environment associated with Pb-O-Cl compounds is now at 138.03eV which indicates an environment that is richer in electron withdrawing species such as chlorine and oxygen. At this higher temperature the Pb 4f environment is dominated by this peak with only minor contributions from Pb at 136.5eV and PbC_2O_4 at 138.85eV. The Cl 2p environment is now at 197.95eV, a small decrease compared to the value measured from the product calcined at 300˚C, but one which could be due to an increase in the number of highly electronegative species nearby that will increase the local electron density of the environment. Secondary electron images show a whisker like morphology that appears to be homogeneous. This morphology is very different to that observed after 300˚C calcination and the numerous rounded surface features seem to suggest that growth of a non-commensurate phase occurred at the crystal surface. These features are highlighted in Figure 12. This could be from the decomposition of $Pb_2Cl_2C_2O_4$ into $Pb_3O_2Cl_2$, or from the reaction of other compounds such as $Pb_5O_2Cl_6$ or $PbCl_2$ with oxygen during the calcination process.

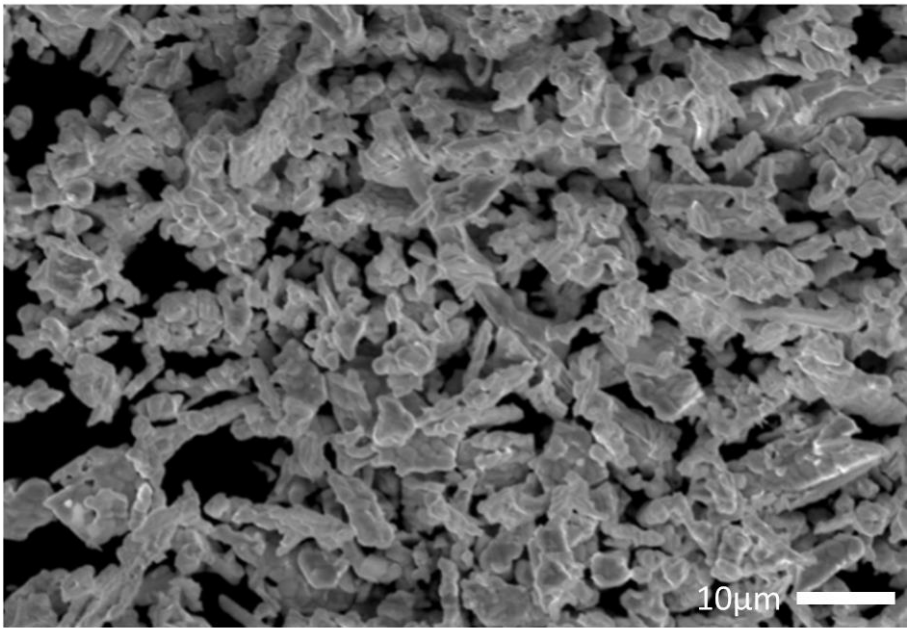

Figure 10: Secondary electron image of chemically converted LAB paste calcined at 500°C.

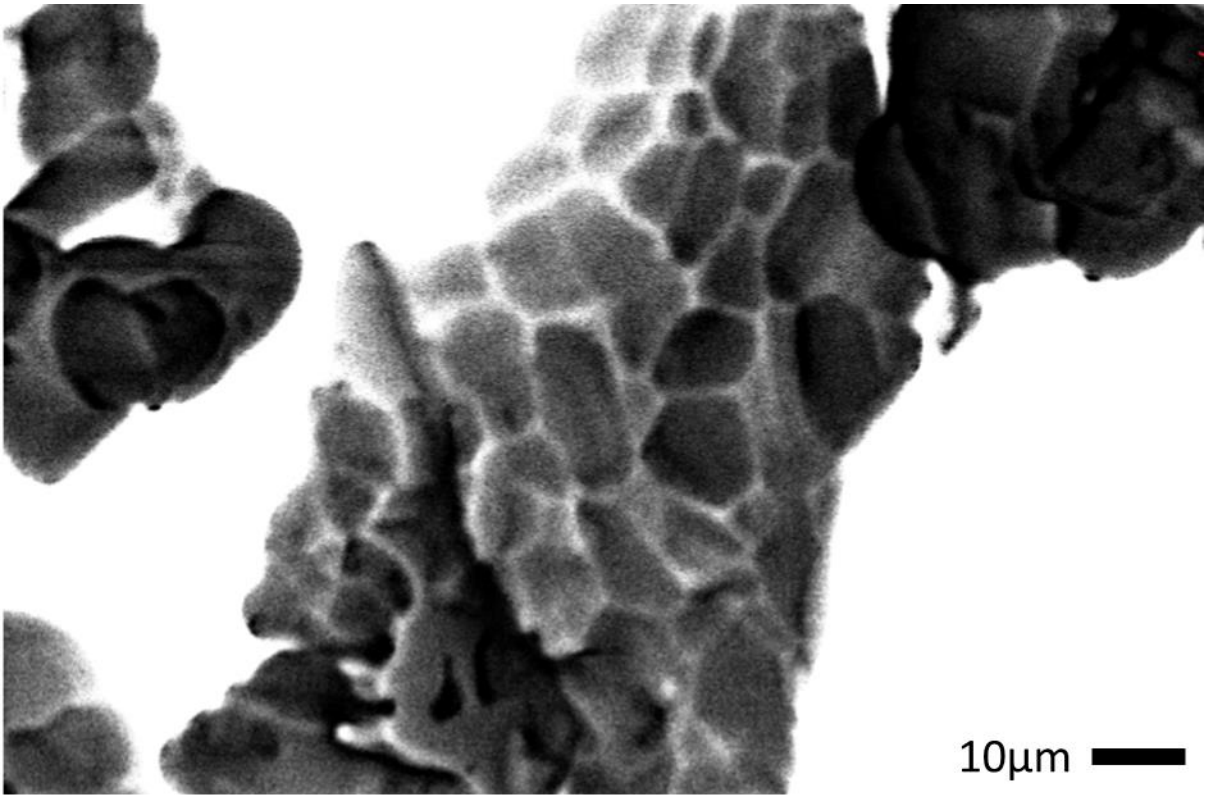

Figure 11: High magnification secondary electron image of growth features found in the sample calcined at 500◦C. Image colours have been inverted and sharpened in post-processing to highlight these features.

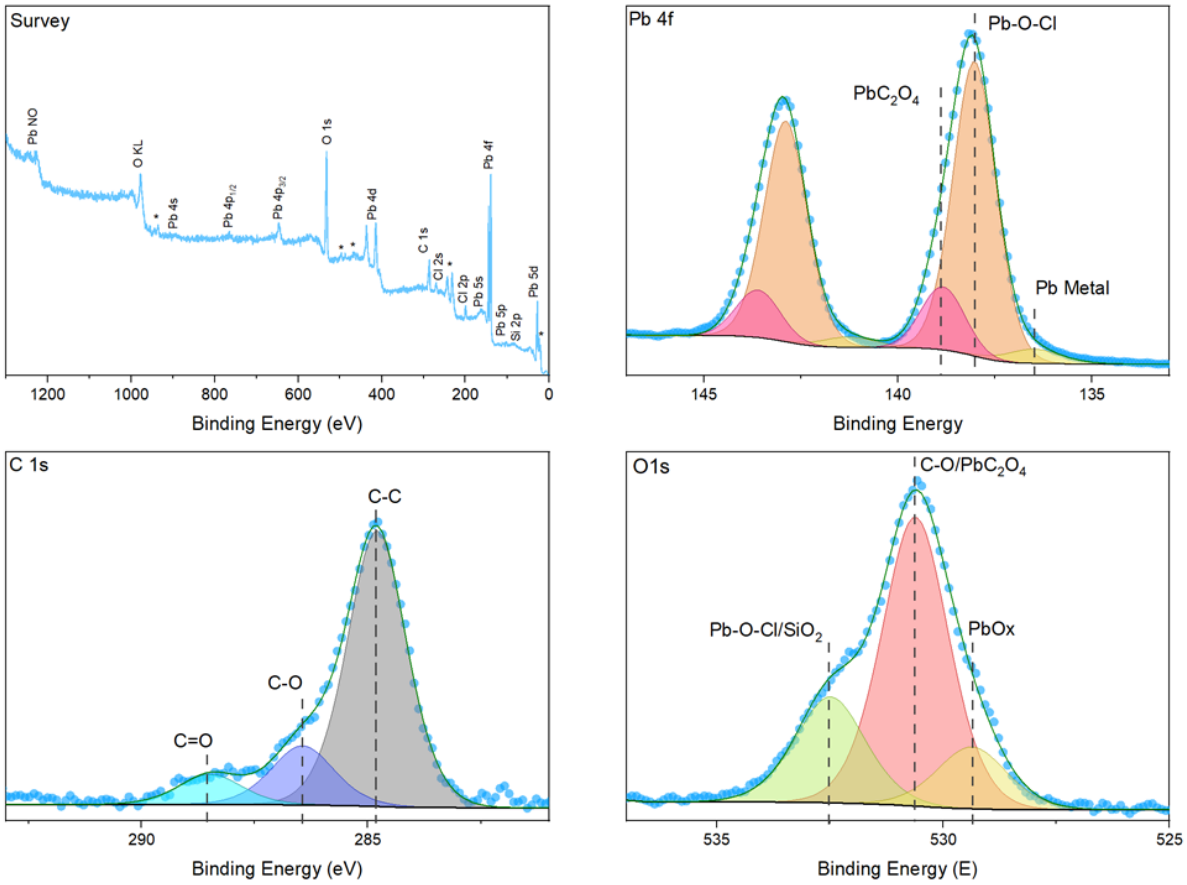

Figure 12: XPS analysis of chemically converted after calcination at 500°C. Survey spectrum of the product showing detected elements. A survey spectrum and core level spectra of Pb4f, C1s and O1s. Data points of core level measurements are shown as blue dots, while the fitted environment peaks are shown as filled areas under the envelope (green).

3.4 Mechanisms of reaction and calcination

When the spent LAB paste is introduced into the oxaline, there is an immediate reaction since some limited effervescence is observed upon addition, with a final white suspension obtained much later. The gas is likely to be CO_2 as it found to extinguish a lit wooden splint. This indicates a two-step reaction (proposed in equations 1 and 2) where first the lead materials are dissolved into the DES system and then react with the oxalic acid hydrogen bond donor ($C_2H_2O_4$), precipitating out of the solution. The unique chemical environment of the DES is thought to promote the availability and reactivity of the Cl anion of the choline chloride ($[C_5H_{14}NO]^+[Cl]^-$) component through a charge de-localisation that occurs between $[C_5H_{14}NO]^+[Cl]^-$ and $C_2H_2O_4$.[29] Increased Cl activity could drive the solution of lead materials into the DES (as observed in previous studies of lead solubility in Ethaline DES)[30] and consequently, $[C_2O_4]^{2-}$ can substitute the Cl^- ligands due to being a more effective chelating agent for the Pb^{2+} ion. [31]

$$PbCO_{3(s)} + 4Cl^-_{(DES)} + 2H^+_{(DES)} \rightarrow [PbCl_4]^{2-}_{(DES)} + CO_{2(g)} + H_2O_{(DES)} \quad (1)$$

$$[PbCl_4]^{2-}_{(DES)} + [C_2O_4]^{2-}_{(DES)} \rightarrow PbC_2O_{4(s)} + 4Cl^-_{(DES)} \quad (2)$$

The identification of $Pb_2Cl_2C_2O_4$ through XRD indicates that another reaction must occur between the chlorine anion and PbC_2O_4. Since $Pb_2Cl_2C_2O_4$ was not found by XPS analysis, it was concluded that this product could form where some DES is trapped between two stacked PbC_2O_4 plates.

This may occur during the cleaning process, when crystals wetted with DES will flocculate due to the DES providing a more favourable surface interaction than the diluent. Prolonged exposure to the DES then leads to the surface PbC_2O_4 crystals to transform into $Pb_2Cl_2C_2O_4$ (as proposed in equation 3).

$$2PbC_2O_{4(s)} + 2Cl^-_{(DES)} \rightarrow Pb_2Cl_2C_2O_4(s) + 2CO_{2(g)} \quad (3)$$

During calcination it is expected that the trapped DES would thermally degrade even at low temperatures. Generally the degradation temperature of a given DES can be estimated as the average of precursor degradation temperatures.[32] Since the decomposition of $[C_5H_{14}NO]^+[Cl]^-$ and $C_2H_2O_4$ happen at 304°C [32] and 150°C [33] respectively, the expected degradation temperature of Oxaline DES is around 230°C. Hence degradation will proceed rapidly during calcination at 300°C and the proposed stoichiometric decomposition pathway is shown in equation 4.

$$2([C_5H_{14}NO]^+ \cdot [Cl]^- \cdot [C_2O_4]^{2-})_{(DES)} \rightarrow 14CO_{2(g)} + Cl_{2(g)} + N_{2(g)} + 14H_2O_{(g)} \quad (4)$$

It is unlikely that the oxygen requirements for stoichiometric decomposition of the DES will be met in ambient air, therefore there may be many products of partial combustion such as CO and intermediate organic substances. As previously discussed, the former is likely responsible for the evolution of metallic lead during calcination, while the latter can confound XPS identification of the final product with overlap in the O 1s core level region. Half a mole of chlorine gas will be evolved per mole of DES decomposed and this could also drive side reactions with other calcination and combustion products. For example, the mineral mendipite can be formed by reacting PbO and $PbCl_2$,[34] where the $PbCl_2$ may be produced by a reaction between Cl_2 and metallic Pb, or PbC_2O_4 as shown in equations 5 and 6.

$$Pb_{(s)} + Cl_{2(g)} \rightarrow PbCl_{2(s)} \quad (5)$$

$$PbC_2O_{4(s)} + Cl_{2(g)} \rightarrow PbCl_{2(s)} + 2CO_{2(g)} \quad (6)$$

As discussed by Boudaren et al.[27] $Pb_2Cl_2C_2O_4$ also has some thermal decomposition pathways that can lead to the formation of $PbCl_2$, $Pb_5O_2Cl_6$ and $Pb_3O_2Cl_2$. It is likely that the kinetics of these mechanisms are slow at temperatures of 300 ºC or below, resulting in very little change as seen in the chemically converted LAB paste calcined at this temperature. However, above this temperature, significant transformations take place as is seen in the specimen calcined at 500°C. In summary, the large amounts of chlorine present in samples during thermal decomposition experiments significantly complicate the degradation behaviour, and lead to the formation of lead oxychloride products as opposed to the expected lead oxides. Further measurements and analysis are needed at intermediate temperatures to fully characterise the transformations taking place within these chemically converted spent LAB paste samples during calcination.

4. Conclusion

Spent LAB paste was chemically converted into a lead oxalate product using an Oxaline DES and subsequently calcined with the aim to thermally decompose the organic lead compound into oxides that are useful for the manufacture of new LABs. Spent LAB paste, chemically converted paste, and the product of calcination at 300°C and 500°C were analysed by PXRD, SEM and XPS. Micron sized silica fibres were found to be present in the starting material and were also shown to persist through all process steps. After chemical conversion some unexpected product in the form of $Pb_2Cl_2C_2O_4$ was found and attributed to prolonged contact of PbC_2O_4 with DES trapped between stacked crystals. This went on to promote the formation of lead oxychloride minerals such as $Pb_3O_2Cl_2$ and $Pb_5O_2Cl_6$ through the generation of free Cl_2 by the thermal decomposition of DES or by the degradation of $Pb_2Cl_2C_2O_4$. The Oxaline conversion process is promising for spent LAB recycling since no energy input other than mixing is required to convert a variety of lead minerals into lead oxalate product. However, the findings of this study indicate that there remain two main challenges in implementing this process industrially. (1) Removing silica fibres from the input stream or during the process. These fibres are insulating and will therefore aversely affect electrode performance if they are recycled into new battery plates along with the recovered oxides. (2) Understanding and controlling the material transformations that lead to the formation of lead oxychloride minerals instead of lead oxides. Oxychloride minerals are not conductive, therefore cannot be used as active mass for new battery manufacture.

5. Acknowledgements

This work was funded by the Reduced Energy Recycling of Lead Acid Batteries (RELAB) project (EP/P004504/1). Enrico Manfredi-Haylock was funded by the EPSRC and Department of Materials through the Science and Solutions for a Changing Planet (SSCP) doctoral partnership hosted by NERC and the Grantham Institute for Climate Change at Imperial College London.

6. References

[1] S. Parissien, *The life of the automobile : a new history of the motor car*. Atlantic Books, 2013.

[2] G. J. May, A. Davidson, and B. Monahov, 'Lead batteries for utility energy storage: A review', *J Energy Storage*, vol. 15, pp. 145–157, Feb. 2018, doi: 10.1016/J.EST.2017.11.008.

[3] International Lead Association, 'Lead Recycling'. Accessed: Apr. 19, 2019. [Online]. Available: https://www.ila-lead.org/UserFiles/File/FS_Recycling.pdf

[4] A. J. Davidson, S. P. Binks, and J. Gediga, 'Lead industry life cycle studies: environmental impact and life cycle assessment of lead battery and architectural sheet production', *Int J Life Cycle Assess*, vol. 21, no. 11, pp. 1624–1636, Nov. 2016, doi: 10.1007/s11367-015-1021-5.

[5] B. Schaddelee-Scholten and J. Tempowski, 'Used Lead Acid Battery Recycling Health Considerations', 2017.

[6] A. G. Betts, 'Art or process of refining lead by electrolysis.', US679824A, 1901

[7] R. David Prengaman, 'Recovering lead from batteries', *JOM*, vol. 47, no. 1, pp. 31–33, Jan. 1995, doi: 10.1007/BF03221127.

[8] J. L. Alvarez, E. Hermana, D. Martin, and F. Martin, 'LEDCLOR process for low grade concentrates and wastes', in *Edited Proceedings Tenth International Lead Conference*, 1990, pp. 156–164.

[9] S. R. Clarke, R. L. Clarke, and B. Dougherty, 'Closed loop systems and methods for recycling lead acid batteires', WO2016183429, Nov. 18, 2016

[10] D. Helm, 'Cost of Energy Review', 2017.

[11] D. Andrews, A. Raychaudhuri, and C. Frias, 'Environmentally sound technologies for recycling secondary lead', *J Power Sources*, vol. 88, no. 1, pp. 124–129, May 2000, doi: 10.1016/S0378-7753(99)00520-0.

[12] M. Volpe *et al.*, 'Metallic lead recovery from lead-acid battery paste by urea acetate dissolution and cementation on iron', *Hydrometallurgy*, vol. 96, no. 1–2, pp. 123–131, Mar. 2009, doi: 10.1016/J.HYDROMET.2008.09.001.

[13] D. Yang *et al.*, 'A novel ultrafine leady oxide prepared from spent lead pastes for application as cathode of lead acid battery', *J Power Sources*, vol. 257, pp. 27–36, Jul. 2014, doi: 10.1016/J.JPOWSOUR.2014.01.091.

[14] WWAP, 'The United Nations world water development report 2019: leaving no one behind', 2019.

[15] A. D. Ballantyne, J. P. Hallett, D. J. Riley, N. Shah, and D. J. Payne, 'Lead acid battery recycling for the twenty-first century', *R Soc Open Sci*, vol. 5, no. 5, p. 171368, May 2018, doi: 10.1098/rsos.171368.

[16] S. yin Tan, D. J. Payne, J. P. Hallett, and G. H. Kelsall, 'Developments in electrochemical processes for recycling lead–acid batteries', *Current Opinion in Electrochemistry*, vol. 16. Elsevier B.V., pp. 83–89, Aug. 01, 2019. doi: 10.1016/j.coelec.2019.04.023.

[17] A. P. Abbott, G. Capper, D. L. Davies, K. J. McKenzie, and S. U. Obi, 'Solubility of metal oxides in deep eutectic solvents based on choline chloride', *J Chem Eng Data*, vol. 51, no. 4, pp. 1280–1282, 2006, doi: 10.1021/je060038c.

[18] A. P. Abbott, G. Frisch, J. Hartley, W. O. Karim, and K. S. Ryder, 'Anodic dissolution of metals in ionic liquids', *Progress in Natural Science: Materials International*, vol. 25, no. 6, pp. 595–602, 2015, doi: 10.1016/j.pnsc.2015.11.005.

[19] C. G. Poll, G. W. Nelson, D. M. Pickup, A. V. Chadwick, D. J. Riley, and D. J. Payne, 'Electrochemical recycling of lead from hybrid organic–inorganic perovskites using deep eutectic solvents', *Green Chemistry*, vol. 18, no. 10, pp. 2946–2955, 2016, doi: 10.1039/C5GC02734A.

[20] D. Pavlov, 'Leady Oxide', in *Lead-Acid Batteries: Science and Technology*, Elsevier, 2017, pp. 245–273. doi: 10.1016/b978-0-444-59552-2.00005-5.

[21] Y. Gong, J. E. Dutrizac, and T. T. Chen, 'The reaction of anglesite (PbSO4) crystals with sodium carbonate solutions', *Hydrometallurgy*, vol. 31, no. 3, pp. 175–199, Nov. 1992, doi: 10.1016/0304-386X(92)90117-I.

[22] J. A. Taylor and D. L. Perry, 'An x-ray photoelectron and electron energy loss study of the oxidation of lead', *Journal of Vacuum Science & Technology A: Vacuum, Surfaces, and Films*, vol. 2, no. 2, pp. 771–774, Apr. 1984, doi: 10.1116/1.572569.

[23] T. Hagio, A. Takase, and S. Umebayashi, 'X-ray photoelectron spectroscopic studies of β-sialons', *J Mater Sci Lett*, vol. 11, no. 12, pp. 878–880, 1992, doi: 10.1007/BF00730493.

[24] K. S. Kim, T. J. O'Leary, and Nicholas. Winograd, 'X-ray photoelectron spectra of lead oxides', *Anal Chem*, vol. 45, no. 13, pp. 2214–2218, Nov. 1973, doi: 10.1021/ac60335a009.

[25] H. Schulte and W. Kirchhoff, 'Lead acid battery plate with starch coated glass fibers', US4238557A, Apr. 20, 1978

[26] V. I. Nefedov, Y. V Salyn, and K. Keller, 'X-ray electron studies of lead and mercury-compounds', *ZHURNAL NEORGANICHESKOI KHIMII*, vol. 24, no. 9. INST OBS NEORG KHIMII IM NS KURNAKOVA LENINSKI PROSPEKT 31, 71 MOSCOW, RUSSIA, pp. 2564–2566, 1979.

[27] C. Boudaren, J.-P. Auffrédic, M. Louër, and D. Louër, 'A powder X-ray diffraction study of lead chloride oxalate Pb2Cl2(C2O4): ab initio structure determination and thermal behavior', *Powder Diffr*, vol. 18, no. 03, pp. 205–213, Sep. 2003, doi: 10.1154/1.1590352.

[28] G. Hope, ‘The influence of oxygen pressure on lead oxidation kinetics’, *Aust J Chem*, vol. 33, no. 3, p. 471, 1980, doi: 10.1071/CH9800471.

[29] M. R. S. J. Foreman, S. Holgersson, C. McPhee, and M. S. Tyumentsev, ‘Activity coefficients in deep eutectic solvents: implications for the solvent extraction of metals’, *New Journal of Chemistry*, vol. 42, no. 3, pp. 2006–2012, Jan. 2018, doi: 10.1039/C7NJ03736H.

[30] C. G. Poll, G. W. Nelson, D. M. Pickup, A. V. Chadwick, D. J. Riley, and D. J. Payne, ‘Electrochemical recycling of lead from hybrid organic–inorganic perovskites using deep eutectic solvents’, *Green Chemistry*, vol. 18, no. 10, pp. 2946–2955, 2016, doi: 10.1039/C5GC02734A.

[31] R. G. Pearson, ‘Hard and Soft Acids and Bases’, *J Am Chem Soc*, vol. 85, no. 22, pp. 3533–3539, Nov. 1963, doi: 10.1021/ja00905a001.

[32] F. Chemat, H. Anjum, A. M. Shariff, P. Kumar, and T. Murugesan, ‘Thermal and physical properties of (Choline chloride + urea + l-arginine) deep eutectic solvents’, *J Mol Liq*, vol. 218, pp. 301–308, Jun. 2016, doi: 10.1016/J.MOLLIQ.2016.02.062.

[33] D. E. Wobbe and W. A. Noyes, ‘Photochemical studies. IV. The thermal decomposition of anhydrous oxalic acid and its relation to the photochemical decomposition’, *J Am Chem Soc*, vol. 48, no. 11, pp. 2856–2868, Nov. 1926, doi: 10.1021/ja01690a015.

[34] O. I. Siidra, S. V Krivovichev, T. Armbruster, and W. Depmeier, ‘Crystal chemistry of the mendipite-type system Pb3O 2Cl2-Pb3O2Br2’, *Zeitschrift fur Kristallographie*, vol. 223, no. 3, pp. 204–211, 2008, doi: 10.1524/zkri.2008.0018.